Available online at www.sciencedirect.com

SCIENCE DIRECT

Thermochimica Acta 443 (2006) 197–205

thermochimica acta

www.elsevier.com/locate/tca

Thermal dehydration of lithium metaborate dihydrate and phase transitions of anhydrous product

Nobuyoshi Koga*, Takahide Utsuoka

Chemistry Laboratory, Graduate School of Education, Hiroshima University, 1-1-1 Kagamiyama, Higashi-Hiroshima 739-8524, Japan

Received 24 December 2005; received in revised form 15 January 2006; accepted 24 January 2006
Available online 28 February 2006

Abstract

Reaction steps and mechanisms of the thermal dehydration of lithium metaborate dihydrate were investigated by means of thermoanalytical measurements, high temperature powder X-ray diffractometry, FT-IR spectroscopy, and microscopic observations. The first half of thermal dehydration was characterized by the melting of the sample producing viscous surface layer, the formation of bubbles on the particle surfaces, and the sudden mass-loss taking place by an opportunity of cracking and/or bursting of the bubble surface layer. The second half of the dehydration with a long-tailed mass-loss process in a wide temperature region was divided further into three distinguished reaction steps by the measurements of controlled rate thermal analysis. During the course of the thermal dehydration, four different poorly crystalline phases of intermediate hydrates were observed, in addition to an amorphous phase produced by an isothermal annealing. Just after completing the thermal dehydration, an exothermic DTA peak of the crystallization of β-$LiBO_2$ was appeared at around 750 K. The phase transition from β-$LiBO_2$ to α-$LiBO_2$ was observed in the temperature range of 800–900 K, which subsequently melted by indicating a sharp endothermic DTA peak with the onset temperature at 1101.4 ± 0.6 K.

Keywords: Lithium metaborate dihydrate; Thermal dehydration; Phase transition; Thermal analysis

1. Introduction

Mechanisms and kinetics of the thermal decomposition of solids have extensively been studied by many workers being exemplified by varieties of the processes from degradation of organic compounds to inorganic ceramic processing. These reactions can be recognized in general as complicated kinetic process which proceeds through interactions of various physical and chemical steps taking place at reaction interface, such as destruction of reactant crystal, breaking of chemical bond, diffusional removal of gaseous product from the reaction front, crystallization of solid products, and so on [1–5]. The actual reaction condition at the reaction front is determined by the reaction itself as a result of such interactions and is influenced markedly by the measuring conditions applied. In addition, the overall rate behavior depends on the geometry of advancement of the reaction front. In order to establish a possible guide of phenomenological interpretation for such complicated reaction processes, it has been attempted to classify the processes by the characteristics of structure of reaction interface and kinetics of the interfacial chemical processes [4,5]. Such an effort of classifying the thermal decomposition processes is expected to contribute notably towards the provision of a theoretical foundation for the further understanding of solid-state reactions. On classifying the thermal decomposition of solids, it has been pointed out that the reaction mechanisms of the processes which produce an amorphous solid as the solid product have not fully been clarified as yet, even though these sometimes exhibit several special reaction behaviors such as pre-melting, sol–gel process, and so on [4,5].

It is known that amorphous anhydrides are obtained as the solid products during the thermal dehydrations of hydrates of alkaline metal and alkaline earth metal borates [6–8]. Through clarifying the reaction mechanisms of the thermal dehydration of a series of the borate hydrates, it is expected that useful information for discussing the characteristics of the reaction behavior producing amorphous products is obtained. For this purpose, kinetics and mechanisms of the thermal dehydrations

---

* Corresponding author.
E-mail address: nkoga@hiroshima-u.ac.jp (N. Koga).

0040-6031/$ – see front matter © 2006 Elsevier B.V. All rights reserved.
doi:10.1016/j.tca.2006.01.029

of $Li_2B_4O_7 \cdot 3H_2O$ and $K_2B_4O_7 \cdot 4H_2O$ have already been investigated [9,10], together with the crystallization behavior of the amorphous products [10–12]. In both the cases, amorphous phases were produced as an intermediate product or dehydration product through the thermal dehydration reactions, where possible participations of a melt or gel phase were presumed. Especially, the overall thermal dehydration process of $K_2B_4O_7 \cdot 4H_2O$ was characterized as a self-induced sol–gel process to form anhydrous glass [10].

Along the same line, the thermal dehydration of lithium metaborate dihydrate, $LiBO_2 \cdot 2H_2O$, is subjected in the present study to investigate the reaction steps and mechanisms by means of thermal analyses, high temperature powder X-ray diffractometry, FT-IR spectroscopy and microscopic observations. It is known that $LiBO_2 \cdot 2H_2O$ is a stable intermediate hydrate obtained during the thermal dehydration of $LiBO_2 \cdot 8H_2O$ [13–16]. In many previous studies [7,13–16], the thermal dehydration process of $LiBO_2 \cdot 2H_2O$ was studied as a part of the thermal dehydration of $LiBO_2 \cdot 8H_2O$, where very complicated phase relations during the course of the thermal dehydration of $LiBO_2 \cdot 2H_2O$ and of phase transitions of anhydrous product were reported. In the present study, single crystalline particles of $LiBO_2 \cdot 2H_2O$, as is shown lately in Fig. 3(a), are subjected for studying the thermal dehydration process from the view point of reaction morphology. It is expected that some new insights into the mechanisms of the thermal dehydration of the title compound are gained by the identification of physico-chemical events through microscopic observations of the selected reaction steps and by the careful separation of the individual reaction steps by means of the controlled rate thermal analysis (CRTA) [17].

2. Experimental

Regent grade lithium metaborate dihydrate (Sigma–Aldrich, Japan) was sieved to various particle-size fractions. The sample was identified by means of powder X-ray diffractometry, FT-IR spectroscopy, and thermogravimetry (TG) and stored for more than 2 weeks before subjecting to various measurements to avoid a possible ageing effect.

Using ca. 10.0 mg of sample weighed onto a platinum crucible of 5 mm in diameter and 2.5 mm in height, the thermal dehydration processes under isothermal and non-isothermal conditions were traced by TG–DTA (ULVAC TGD9600) in flowing N_2 at a rate of 80 $cm^3\,min^{-1}$. Measurements of CRTA were also performed using an instrument of TG (Shimadzu TGA50) equipped with a self-constructed CRTA controller [17–19], where the mass-loss rate during the course of dehydration reaction was controlled to be a constant value of 10.0 $\mu g\,min^{-1}$.

Textural changes during the thermal dehydration were observed using a reflection microscope (Olympus BH2) with a programmable heating stage (Linkam TH600). Observations of typical textures of the samples at several selected reaction steps were made by using a scanning electron microscope (SEM, Jeol JSM-T20) after coating the samples by Au evaporation.

The phase changes during the thermal dehydration process were followed by high-temperature powder X-ray diffractometer (Rigaku RINT2200V) equipped with a heating chamber (Rigaku TC20) using monochrome Cu Kα radiation (40 kV, 20 mA). FT-IR spectra for the samples heated linearly to various temperatures were recorded by diffuse reflectance method (Shimadzu FTIR8100M) after diluting the sample with KBr powder.

3. Results and discussions

3.1. Overall reaction behavior and reaction morphologies

Fig. 1 shows typical TG–DTA curves for the thermal dehydration of $LiBO_2 \cdot 2H_2O$ at a heating rate ($\beta = 10\,K\,min^{-1}$) under flowing N_2 (80 $cm^3\,min^{-1}$). The total mass-loss of 41.9 ± 0.3% recorded on TG was in good agreement with the theoretical value (42.0%) calculated by assuming the following dehydration reaction: $LiBO_2 \cdot 2H_2O \rightarrow LiBO_2 + 2H_2O$. The overall behavior of the dehydration process is characterized by a rapid mass-loss process corresponding to an endothermic DTA peak at around 430 K and subsequent long-tailed mass-loss steps in a wide temperature region up to 700 K. Just after completing the mass-loss process, an exothermic DTA peak was detected at around 725–800 K. On further heating, a sharp endothermic DTA peak appears with the onset temperature at 1101.4 ± 0.6 K and peak top temperature at 1120.5 ± 1.3 K, which corresponds closely to the reported melting point of α-$LiBO_2$ [20,21].

Detailed observation of the TG–DTA curves in Fig. 1 reveals that small but detectable shoulders exist at the very beginning of the dehydration reaction. Fig. 2 compares the DTG curves recorded under flowing N_2 (80 $cm^3\,min^{-1}$) at a heating rate of 2 $K\,min^{-1}$ for the early stage of the dehydration of the samples with different particle sizes. Irrespective of the particle sizes, a small DTG peak is observed at the beginning of the dehydration reaction. Because the sample with the smaller particle size indicates the larger DTG peak, the DTG peak is expected to result from the surface reaction. The mass-loss rate is decelerated after

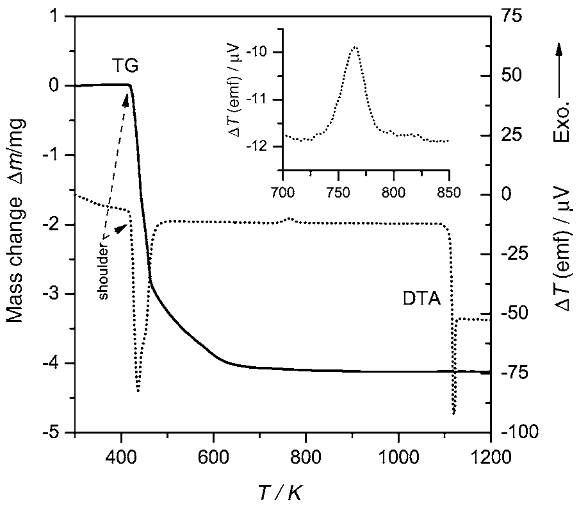

Fig. 1. Typical TG–DTA curves for the thermal dehydration of $LiBO_2 \cdot 2H_2O$ (10.0 mg, −100 + 170 mesh) at a heating rate ($\beta = 10\,K\,min^{-1}$) under flowing N_2 (80 $cm^3\,min^{-1}$).

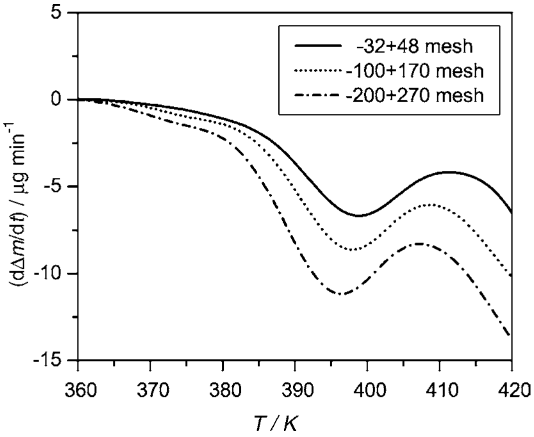

Fig. 2. Comparison of DTG curves for the early stage of thermal dehydration of $LiBO_2 \cdot 2H_2O$ (10.0 mg) with different fractions of particle sizes.

the surface reaction and subsequently accelerated suddenly with a large endothermic DTA peak, see Fig. 1. The separated DTG peak for the surface reaction indicates that switching from the surface reaction to the subsequent established reaction does not proceed smoothly, due to possible interruption of diffusional removal of product water vapor produced by internal reaction. The surfaces of sample particles are very sticky during the early stage of the reaction, possibly due to surface melting promoted by an interaction between the surface product layer and water vapor produced by the internal reaction.

Drastic increase in the apparent volume of the assemblage of the sample particles is alternative characteristic of the early stage of the reaction. Fig. 3 shows typical microscopic views of the early stage of the thermal dehydration process of the sample particles observed by heating linearly at a rate of 2 K min^{-1}. At the very beginning of the reaction, melting of the sample surfaces is observed; Fig. 3(b). Subsequently, bubbles are formed on the surface of the sample particles; Fig. 3(c). It is understand that the apparent volume increase of the assemblage of sample particles during the thermal dehydration process is ascribed to the formation of the bubbles on the surface of the sample particles, result from the blocking action of the diffusional removal of the water vapor by the viscous surface layer and the consequent increase in the internal pressure due to the water vapor produced by the internal reaction.

Fig. 4 shows a typical SEM micrograph for the sample heated linearly at a rate of 2 K min^{-1} to 400 K, i.e. the top of the DTA endothermic peak for the dehydration process. The abrupt mass-loss just after the surface process seems to take place by an opportunity of cracking and/or bursting of the bubble surface layer. The hole observed on the bubble surface in the SEM micrograph is an evidence of such reaction behavior. It can also be seen that the internal of the outer layer comes hollow. This indicates that the melting of the sample also takes place in the internal of the sample particles, which subsequently dehydrate by increasing water vapor pressure inside of the melted viscous sample particles and by educing the intermediate solid product at the inside of the expanded surface layer.

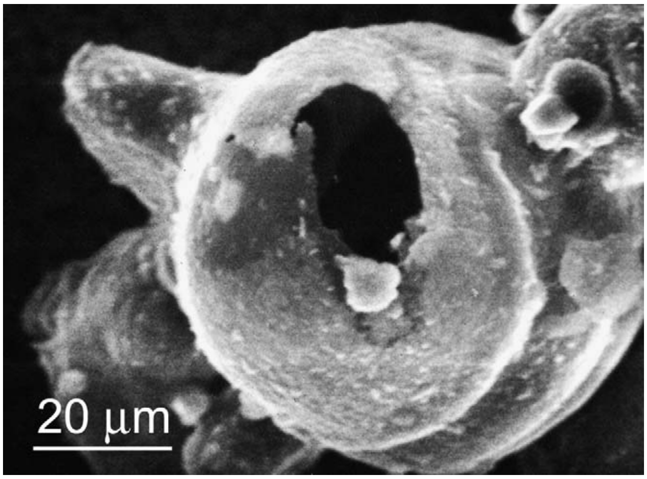

Fig. 4. A typical SEM micrograph of the sample particle heated linearly at a rate of 2 K min^{-1} to 400 K.

3.2. Phase changes in the course of reaction

Fig. 5 shows the changes of the powder X-ray diffraction (XRD) patterns of the sample during heating from room temperature to just below the melting point at a heating rate of 10 K min^{-1} under flowing N_2 (100 cm^3 min^{-1}), where the temperature was kept constant during the XRD measurements for 10 min. Five different powder XRD patterns were observed during heating the sample. At room temperature, the powder XRD pattern corresponds perfectly to $LiBO_2 \cdot 2H_2O$ [15,16,22–24]; Fig. 5(a). A very poorly crystalline phase of the partially dehydrated intermediate was produced in the temperature range from 423 to 523 K; Fig. 5(b). The temperature range is corresponding

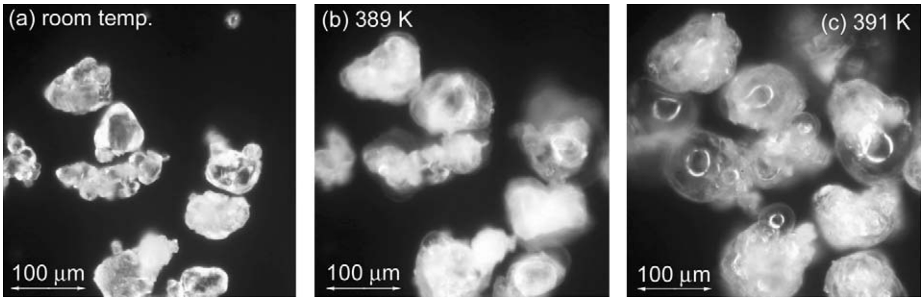

Fig. 3. Typical microscopic views of the early stage of the thermal dehydration of $LiBO_2 \cdot 2H_2O$ particles (−32 + 48 mesh) observed at a heating rate of 2 K min^{-1} under flowing N_2 (80 cm^3 min^{-1}).

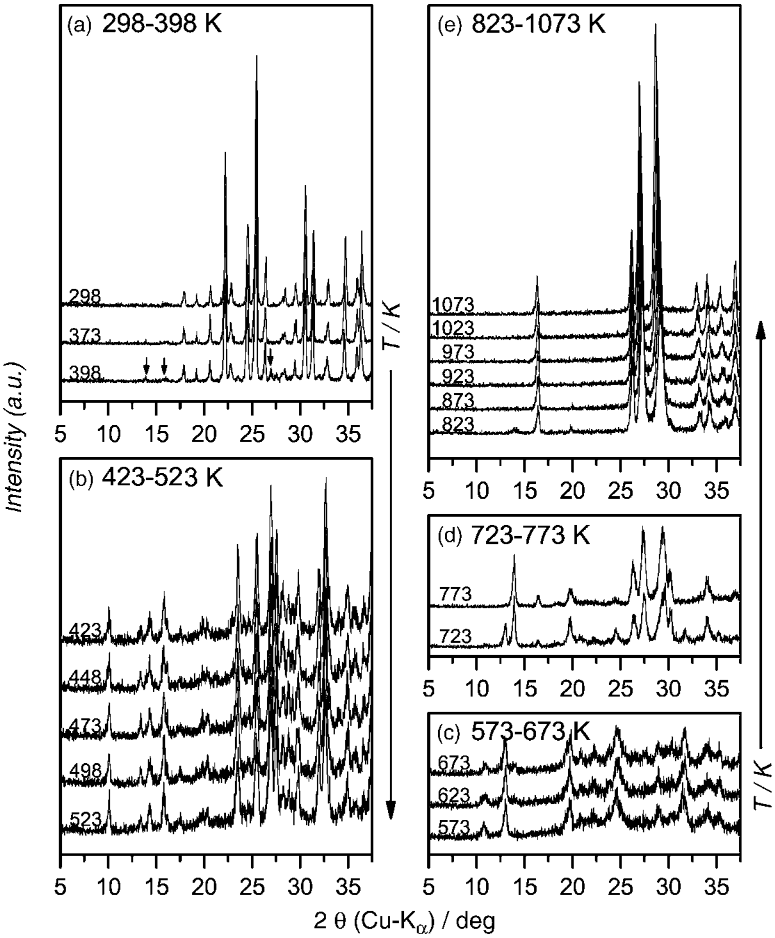

Fig. 5. Changes of the powder X-ray diffraction patterns of the sample during stepwise heating at a heating rate of 10 K min^{-1} and holding for 10 min for diffraction measurements at various temperatures.

to the first half dehydration stage with abrupt mass-loss process. The powder XRD pattern observed at this stage is very close to that reported by Bouaziz as $LiBO_2{\cdot}0.5H_2O$ [25,26]. In the previous studies [15,16], formation of an amorphous phase was reported at this dehydration stage, instead of the presently observed poorly crystalline phase. Although the formation of an amorphous phase may be expected from the melting of the sample, present result indicates that the poorly crystalline phase is directly produced from crystalline $LiBO_2{\cdot}2H_2O$, because several XRD peaks attributed to the partially dehydrated phase are observed at the very beginning of the dehydration reaction as indicated in the powder XRD pattern at 398 K, Fig. 5(a). The difference in the produced phase at the early stage of the dehydration seems to result from the heating conditions applied. Slow heating rates at slower than 0.3 K min^{-1} were applied in the previous studies [15,16].

A different poorly crystalline phase of further dehydrated sample was observed in the temperature range from 573 to 673 K as shown in Fig. 5(c), where the long-tailed mass-loss behavior is observed in the TG–DTA curves shown in Fig. 1. The powder XRD pattern observed at this stage is similar to that reported as $LiBO_2{\cdot}0.3H_2O$_I by Betourne and Touboul [16]. After completing the mass-loss due to dehydration, a phase transition is observed in the temperature range from 723 to 773 K; Fig. 5(d). The temperature range is corresponding to that of the exothermic DTA peak observed in Fig. 1. The powder XRD pattern of the product phase corresponds to that attributed to β-$LiBO_2$ [27]. Formation of β-$LiBO_2$ at around 750 K has been reported by Betourne and Touboul [16], while the corresponding phase has not been identified by Liang et al. [15]. On further heating, β-$LiBO_2$ transforms to α-$LiBO_2$ [16,28,29] between 773 and 873 K, Fig. 5(e). Above 923 K, no distinguished XRD peak due to β-$LiBO_2$ can be detected and the intensities of the powder XRD peaks attributed to α-$LiBO_2$ increase gradually with increasing temperature.

FT-IR spectra for the samples heated linearly (10 K min^{-1}) to various temperatures were shown in Fig. 6. The absorption peak between 2800 and 3850 cm^{-1} attributed to the O–H stretching vibration [30] is attenuated in the temperature range of the thermal dehydration, ∼623 K. The symmetric stretching mode of four-coordinated borate observed between 800 and 1100 cm^{-1} [13,15,20,31,32] remains up to 873 K and disappears completely at the higher temperatures. The stretching mode of BO_4 is a broad envelope in the temperature range of thermal dehydration and is separated into several peaks at the higher temperatures. Continuous growth of the absorption peaks attributed to three-coordinated BO_3 group, i.e. 450–800 and 1100–1600 cm^{-1} [13,15,20,31,32], is observed during the course of the heat treat-

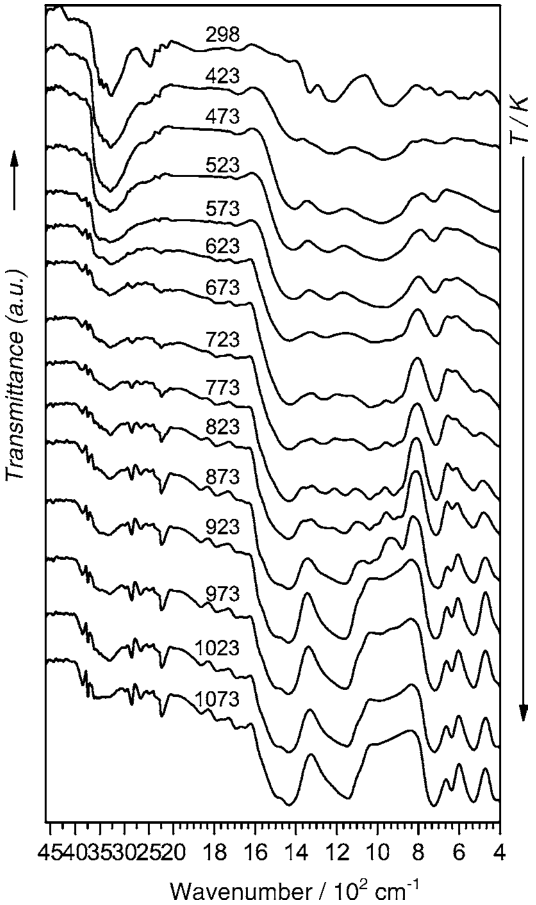

Fig. 6. FT-IR spectra for the samples heated at a heating rate of 10 K min^{-1} to various temperatures.

ment. Accordingly, the three- and four-coordinated borate anion groups exist in the temperature region lower than 873 K, while only the three-coordinated borate anion can be found at the higher temperature. Although the crystal structure of β-$LiBO_2$ has not been determined as yet, it is known that the phase indicates the IR absorption peaks due to three- and four-coordinated borates [13]. Formation of β-$LiBO_2$ by the exothermic phase transition at around 750 K is thus supported also by the FT-IR spectra within the temperature range of 723–873 K. As was conformed by the powder XRD measurements, β-$LiBO_2$ transforms subsequently to α-$LiBO_2$, built from a chain of BO_3 triangles [13,28,29].

3.3. Reaction steps of the thermal dehydration by CRTA

In order to trace thermoanalytically the thermal dehydration processes in some more details with the higher resolution, about 10 mg of the sample was subjected to the measurements of CRTA under flowing N_2 (80 cm^3 min^{-1}), where the reaction temperature was regulated automatically so as to control the mass-loss rate during the course of dehydration reaction to be a constant value of 10.0 μg min^{-1}. Fig. 7 shows typical CRTA record for the sample (9.52 mg of −100 + 170 mesh). It can be clearly seen that the thermal dehydration processes can be divided into four different reaction steps with separated profiles of reaction temperature curves designated as I–IV in Fig. 7. The reaction step I proceeds at constant temperature, indicating the zero order kinetic behavior [18,33–35]. A small DTG peak is observed at the very beginning of the reaction step I, followed by the rapid increase in the reaction rate indicating an overshooting in the reaction rate control. The behavior is in good agreement with the conventional TG–DTA in Fig. 1 and is characterized by the melting of the sample and the dehydration from the viscous sample particles. The fluctuations of the controlled reaction rate observed at the early stage of the reaction step seems to be due to the bubbling observed microscopically in Figs. 3 and 4. The mass-loss of about 25% observed for the reaction step I corresponds to the loss of ca. 1.2 mol water molecules in the formal chemical equation.

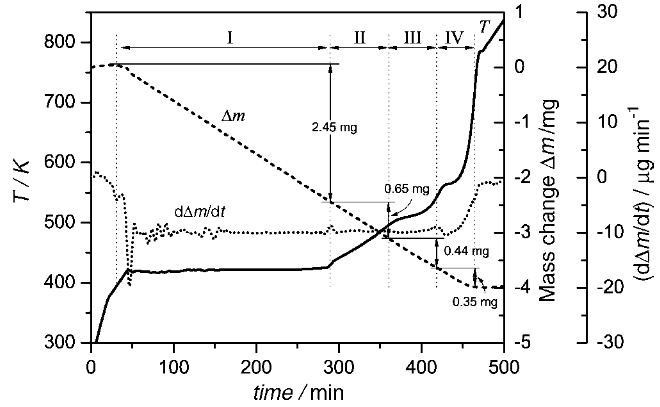

Fig. 7. A typical CRTA record for the sample (9.52 mg of −100 + 170 mesh) at a constant mass-loss rate of 10 μg min^{-1} under flowing N_2 (80 cm^3 min^{-1}).

At the boundary between reaction steps I and II, the reaction temperature starts to increase suddenly, which seems to indicate the solidification of the viscous reactant by the thermal dehydration. The nearly linear increase in the reaction temperature is characteristic for the reaction step II. The total mass-loss of reaction steps I and II attains to about 30%, which corresponds to the loss of 1.5 mol water molecules in the formal chemical equation. The reaction temperature curve turns to a constant temperature at around 510 K for the reaction step III and increase linearly at the end of reaction step III. The temperature range of reaction steps II and III corresponds to that of the formation of the poorly crystalline phase shown in Fig. 5(b). The fractional dehydration is about 90% at the end of the reaction step III. Subsequently, the temperature curve indicates a sigmoid in the temperature range from 550 to 700 K for the reaction step IV. The temperature range of the reaction step IV corresponds to another poorly crystalline phase shown in Fig. 5(c). The profile of the temperature curve observed for the reaction step IV resembles in the shape to that for the diffusion controlled reaction [18,34,35]. The crystal structure observed in the temperature range of the reaction step IV is maintained up to the exothermic phase transition taking place at the end of the dehydration process.

3.4. Isothermal treatment of the sample

Fig. 8 shows typical isothermal mass-loss traces for the thermal dehydration of $LiBO_2 \cdot 2H_2O$ (−100 + 170 mesh) at various

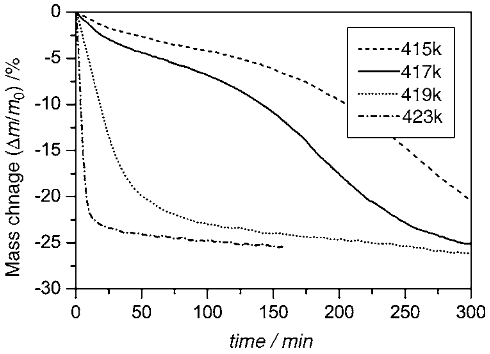

Fig. 8. Typical isothermal mass-loss traces for the thermal dehydration of $LiBO_2 \cdot 2H_2O$ (−100 + 170 mesh) at various constant temperatures under flowing N_2 (80 $cm^3\ min^{-1}$).

constant temperatures. The mass-loss values of the isothermal dehydration at different temperatures are closely correlated to that observed for the reaction step I in Fig. 7. It is worth noting that the shapes of the isothermal mass-loss traces change between those at 417 and 419 K. At the lower temperature than the boundary temperature, the mass-loss is taking place by the two separated reaction steps, while at the higher temperature the reaction proceeds smoothly up to about 20% of mass-loss by accompanying the subsequent long tail.

By taking account the differences of the isothermal reaction behaviors, the sample of −100 + 170 mesh was annealed isothermally at constant temperatures of 413 and 427 K for 24 h under flowing N_2 (100 $cm^3\ min^{-1}$). The values of total mass-loss during the isothermal treatments were 27.8 and 28.7% for the samples annealed at 413 and 427 K, respectively. Fig. 9 compares the powder XRD patterns of intermediate products obtained by the above isothermal treatments at 413 and 427 K. For the sample annealed isothermally at 413 K, a XRD pattern of poorly crystalline phase was obtained, which is different from the intermediate hydrated phases observed in Fig. 5 and from the intermediate phase reported as $LiBO_2 \cdot xH_2O$ by Betourne and Touboul [16]. On the other hand, no distinguished XRD peak is observed for the sample heated at 427 K. Formation of an amorphous intermediate hydrate by the isothermal treatment in the corresponding temperature range has been reported in the previous studies [15,16]. Although Liang et al. [15] reported the existence of the diffraction ring of $d = 3.49$ Å in the powder XRD pattern for the amorphous intermediate, the amorphous phase obtained in the present work dose not indicate the corresponding diffraction ring, see Fig. 9(b).

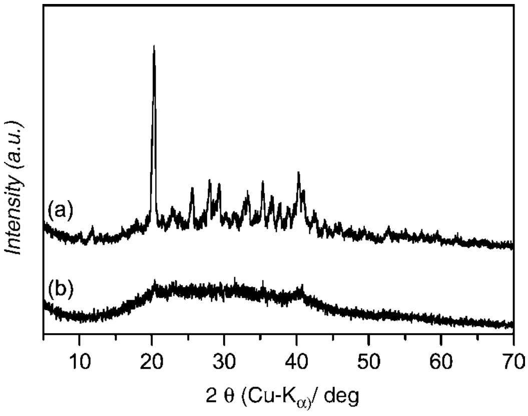

Fig. 9. Typical powder X-ray diffraction patterns of the intermediate hydrates obtained by annealing the samples (−100 + 170 mesh) isothermally at (a) 413 K and (b) 427 K for 24 h under flowing N_2 (80 $cm^3\ min^{-1}$).

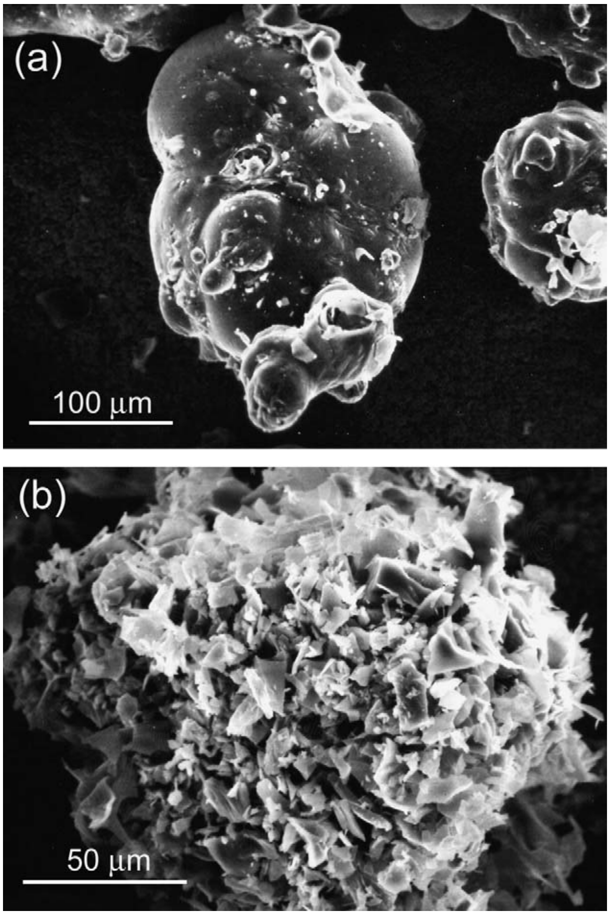

Fig. 10. Typical SEM micrographs of the intermediate hydrates produced by annealing the samples (−100 + 170 mesh) isothermally at (a) 413 K and (b) 427 K for 24 h under flowing N_2 (80 $cm^3\ min^{-1}$).

Fig. 10 shows typical SEM micrographs for the intermediate hydrates produced by heating the samples isothermally at 413 and 427 K for 24 h. The intermediate hydrate produced at 413 K, Fig. 10(a), swells out like a balloon forming a smooth surface. In contrast, as for the intermediate hydrate produced at 427 K, Fig. 10(b), finely destructed pieces of the intermediate solid product stick to the expanded sample surface and disperse elsewhere. The different reaction morphologies seem to result from the change in the viscosity of the melted reactant and the increasing rate of internal water vapor pressure depending on the reaction temperature. In the isothermal treatment at 413 K, the internal water vapor pressure is likely to increase at a moderate rate, resulting in the well-shaped balloon. The dehydration from the viscous reactant of balloon surfaces is also expected to proceed at a moderate rate, allowing the nucleation of poorly crystalline intermediate phase. In comparison, the internal water vapor pressure increases at the higher rate during the isothermal

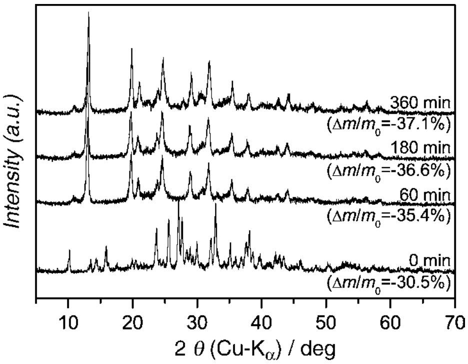

Fig. 11. Changes of the powder X-ray diffraction patterns by the isothermal annealing at 523 K.

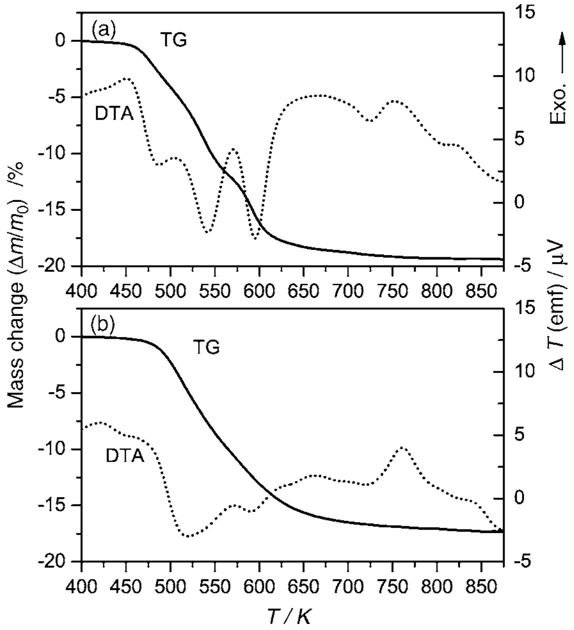

Fig. 12. Typical TG–DTA curves for the intermediate hydrates (10.0 mg), produced by the isothermal annealing of the samples at (a) 413 K and (b) 427 K, at a heating rate of 10 K min^{-1} under flowing N_2 (80 cm^3 min^{-1}).

treatment at 427 K. The bubbling and the bursting of the bubbles enhanced by the higher water vapor pressure are deduced from the destructed pieces of the solidified bubble surfaces, Fig. 10(b). The higher rate of the dehydration from the viscous reactant is one of the most probable reasons for the formation of amorphous intermediate.

For finding different crystalline phases of intermediate hydrate, the sample was subject to the isothermal annealing at several selected temperature ranging from 473 to 773 K under flowing N_2 (100 cm^3 min^{-1}), after heating to the temperature at 10 K min^{-1}. Another poorly crystallized phase was found during the isothermal annealing at 523 K. Fig. 11 shows the changes of the powder XRD patterns with the annealing time at 523 K. By the linear heating to 523 K, the poorly crystallized phase designated as $LiBO_2{\cdot}0.5H_2O$ is produced as was seen in Fig. 5. The powder XRD pattern changes within 60 min to that corresponds to the previously reported phase designated as $LiBO_2{\cdot}xH_2O$ by Betourne and Touboul [16]. No other new phase of intermediate hydrate was found by the isothermal annealing.

3.5. Thermal behaviors of the partially dehydrated intermediate phases

The thermal behaviors of the intermediate hydrates produced through the isothermal treatments at 413 and 427 K were traced

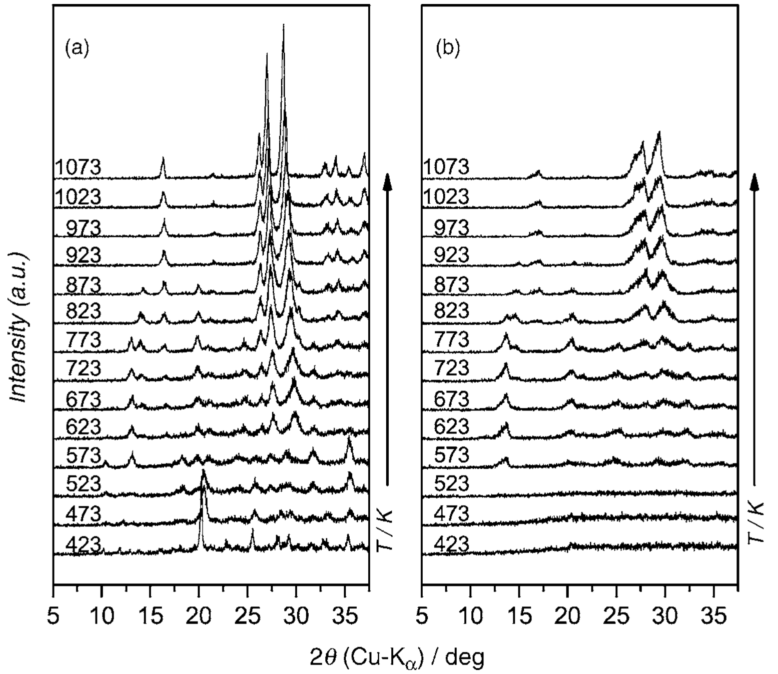

Fig. 13. Changes of the powder X-ray diffraction patterns of the intermediate hydrates, produced by the isothermal annealing of the samples at (a) 413 K and (b) 427 K, during stepwise heating at a heating rate of 10 K min^{-1} and holding for 10 min for diffraction measurements at various temperatures.

by means of TG–DTA and powder XRD measurements. Fig. 12 shows typical TG–DTA curves for the intermediate hydrates (ca. 10 mg) recorded at a heating rate of 10 K min^{-1} under flowing N_2 (80 ml min^{-1}). As for the poorly crystalline intermediate hydrate obtained by heating isothermally at 413 K, Fig. 12(a), three distinguished dehydration steps with endothermic peaks were observed during heating up to 650 K, which are corresponding to the reaction steps II–IV identified in Fig. 7. Another endothermic mass-loss step is observed at around 725 K, just before the exothermic DTA peak of β-$LiBO_2$ formation. After the exothermic DTA peak of β-$LiBO_2$ formation, a small exothermic DTA peak, which was not detected in Fig. 1, is observed.

The mass-loss steps are not clearly separated for the amorphous intermediate hydrate obtained by the isothermal treatment at 427 K, see Fig. 12(b). The endothermic DTA peaks of the dehydration steps are largely overlapped, indicating broad endothermic effect in the temperature range from 400 to 700 K. Two distinguished exothermic DTA peaks in the temperature range above 700 K can be seen as is the case of the poorly crystalline intermediate hydrate obtained by the isothermal treatment at 413 K.

Changes of the powder XRD patterns during the stepwise heating of the intermediate hydrates obtained by the isothermal treatments at 413 and 427 K were shown in Fig. 13. As can be seen in Fig. 13(a), the poorly crystalline intermediate hydrate transforms directly to the phase designated as $LiBO_2 \cdot 0.3H_2O\_I$ [16] at around 573 K. The transformation from $LiBO_2 \cdot 0.3H_2O\_I$ to β-$LiBO_2$ is taking place in the temperature range from 673 to 773 K, corresponding to that of the partially overlapped endothermic and exothermic DTA peaks observed in Fig. 12(a). In the temperature range of the second exothermic DTA peak in Fig. 12(a), the powder XRD pattern of the sample changes from β-$LiBO_2$ to α-$LiBO_2$.

The amorphous intermediate phase obtained by the isothermal treatment at 427 K does not indicate any XRD peaks on heating up to 523 K. A very poorly crystalline phase similar to $LiBO_2 \cdot 3H_2O\_I$ appears at 573 K. Although the sample transforms to α-$LiBO_2$ via β-$LiBO_2$ on further heating as is the case of the poorly crystalline phase obtained by the isothermal treatment at 413 K, the crystallinities of all the appeared phases are very poor compared with those observed during the stepwise heating of $LiBO_2 \cdot 2H_2O$, Fig. 5, and of the crystalline intermediate phase obtained by the isothermal treatment at 413 K, Fig. 13(a).

4. Conclusions

The thermal dehydration of single crystalline particles of $LiBO_2 \cdot 2H_2O$ initiates by the melting of the sample at around 380 K producing viscous surface layers. The sample particles swell out forming bubbles due to the increase of the internal water vapor pressure produced by the internal reaction. Subsequently, the reaction turns to an abrupt mass-loss step by an opportunity of cracking and/or bursting of the bubbles. The reaction behavior of the early stage of the dehydration reaction changes depending on the heating condition. By heating isothermally at the lower than 417 K, the dehydration proceeds by keeping the shape of bubbles and a poorly crystalline intermediate hydrate is produced. At a constant temperature higher than 419 K, the bubbles are destructed finely through the reaction step and an amorphous intermediate hydrate is produced.

By the CRTA measurement for $LiBO_2 \cdot 2H_2O$ and the TG–DTA of the intermediate hydrates obtained by the isothermal treatment of the sample, it was clarified that the second half of the dehydration process with a long-tailed mass-loss is divided further into three distinguished mass-loss steps. Two different poorly crystalline phases of intermediate hydrates were detected during the course of the second half of the dehydration process, which correspond to the previously reported phases designated as $LiBO_2 \cdot 0.5H_2O$ and $LiBO_2 \cdot 0.3H_2O\_I$. Another crystalline phase of intermediate hydrate designated as $LiBO_2 \cdot xH_2O$ was found by annealing the phase $LiBO_2 \cdot 0.5H_2O$ isothermally at 523 K. Totally, four different poorly crystalline phases and an amorphous phase of intermediate hydrates were detected in the present study during the thermal dehydration of $LiBO_2 \cdot 2H_2O$.

Just after completing the dehydration, β-$LiBO_2$ crystallizes in the temperature range from 700 to 800 K with an exothermic DTA peak. On further heating, β-$LiBO_2$ transforms to α-$LiBO_2$ with an exothermic DTA peak at the temperature higher than 800 K. The melting of α-$LiBO_2$ is observed at around 1101.4 ± 0.6 K.

References

[1] D.A. Young, Decomposition of Solids, Pergamon, Oxford, 1966.
[2] M.E. Brown, D. Dollimore, A.K. Galwey, Reactions in the Solid State, Elsevier, Amsterdam, 1980.
[3] A.K. Galwey, M.E. Brown, Thermal Decomposition of Ionic Solids, Elsevier, Amsterdam, 1999.
[4] A.K. Galwey, Thermochim. Acta 355 (2000) 181.
[5] N. Koga, H. Tanaka, Thermochim. Acta 388 (2002) 41.
[6] M. Touboul, E. Betourne, Solid State Ionics 63–65 (1993) 340.
[7] M. Touboul, E. Betourne, Solid State Ionics 84 (1996) 189.
[8] M. Touboul, N. Penin, G. Nowogrocki, Solid State Sci. 5 (2003) 1327.
[9] N. Koga, J.M. Criado, H. Tanaka, J. Therm. Anal. Calorim. 67 (2002) 153.
[10] N. Koga, T. Utsuoka, H. Tanaka, J. Therm. Anal. Calorim. 80 (2005) 71.
[11] N. Koga, K. Yamaguchi, J. Sestak, J. Therm. Anal. Calorim. 56 (1999) 755.
[12] N. Koga, J. Sestak, J. Am. Ceram. Soc. 83 (2000) 1753.
[13] C. Martin, Verres Refract. 40 (1986) 536.
[14] M. Touboul, E. Betourne, G. Nowogrocki, J. Solid State Chem. 115 (1995) 549.
[15] J. Liang, X. Chen, J. Min, Z. Chai, S. Zhao, X. Cheng, Y. Zhang, G. Rao, Phys. Rev. B 51 (1995) 756.
[16] E. Betourne, M. Touboul, Powder Diffr. 12 (1997) 155.
[17] O.T. Sorensen, J. Rouquerol (Eds.), Sample Controlled Thermal Analysis, Kluwer, Dordrecht, 2003.
[18] N. Koga, J.M. Criado, H. Tanaka, Netsu Sokutei 27 (2000) 128, in Japanese.
[19] N. Koga, J.M. Criado, H. Tanaka, J. Therm. Anal. Calorim. 60 (2000) 943.
[20] G.D. Cryssikos, J.A. Kapoutsis, E.I. Kamitsos, A.P. Patsis, A.J. Pappin, J. Non-Cryst. Solids 167 (1994) 92.
[21] M.D. Mathews, A.K. Tyagi, P.N. Moorthy, Thermochim. Acta 320 (1998) 89.
[22] JCPDS 44-0419.
[23] E. Hohne, Z. Anorg. Allg. Chem. 342 (1966) 188.

[24] M. Touboul, E. Betourne, B. Gerand, Powder Diffr. 9 (1994) 54.
[25] R. Bouaziz, Bull. Soc. Chim. Fr. 7 (1962) 1451.
[26] JCPDS 16-0198.
[27] Y. Song, Z. Huang, Mater. Lett. 12 (1991) 363.
[28] W.H. Zachariasen, Acta Cryst. 17 (1964) 749.
[29] A. Kirfel, G. Will, R.F. Stewart, Acta Cryst. B39 (1983) 175.
[30] K. Nakamoto, Infrared Spectra of Inorganic and Coordination Compounds, 2nd ed., Wiley, New York, 1970.
[31] P.B. Hart, J. Inorg. Nucl. Chem. 24 (1962) 1047.
[32] C.E. Weir, R.A. Schroeder, J. Res. Natl. Bur. Stand. 68A (1964) 465.
[33] N. Koga, H. Tanaka, Thermochim. Acta 209 (1992) 127.
[34] J.M. Criado, A. Ortega, F. Gotor, Thermochim. Acta 151 (1990) 171.
[35] L.A. Perez-Maqueda, A. Ortega, F. Gotor, Thermochim. Acta 277 (1996) 165.